STRAIN RATE EFFECT ON THE FATIGUE FAILURE OF THIN PVD COATINGS: AN INVESTIGATION BY A NOVEL IMPACT TESTER WITH ADJUSTABLE REPETITIVE FORCE

K.-D. Bouzakis[1,2], G. Maliaris[1,2], S. Makrimallakis[1,2]

1. *Laboratory for Machine Tools and Manufacturing Engineering, Mechanical Engineering Department, Aristoteles University of Thessaloniki, Greece*
2. *Fraunhofer Project Center Coatings in Manufacturing, in Centre for Research and Technology Hellas (CERTH) GR-57001 Thessaloniki and in Fraunhofer Institute for Production Technology (IPT) D-52074 Aachen Germany*

ABSTRACT

Physical vapor deposition (PVD) coated surfaces are often subjected to repetitive impact loads. In such cases, the strain rate's effect on the coating fatigue failure is pivotal. This effect was investigated via a novel impact tester which facilitates the modulation of the applied impact force versus the time through an adjustable piezoelectric actuator. Using the developed test arrangement, impact loads of various patterns, frequencies and durations were generated and the coated specimens' surface response and film fatigue fracture were captured. Based on these results, it was possible to correspond impact forces of various data to equivalent quasi static ones which induce approximately the same coating and substrate deformation. At the latter loads, the coated specimen deformation was determined by Finite Element Method (FEM) calculations taking into account elastic – plastic film and substrate properties attained by an analytical evaluation of nanoindentation results. Moreover, strain, strain rate combinations insuring film fatigue endurance after one million impacts were estimated.

KEYWORDS: Impact test, modulated force, film fatigue endurance, strain, strain rate

1. INTRODUCTION

Coated surfaces are often subjected to repetitive impact loads. Characteristic examples represent coated surfaces of bearing rings, cutting tools, machine elements etc.. In such applications, since the impact load on a coated surface may possess duration of approximately few microseconds up to several decades of milliseconds, strain rate's effect on the film fatigue failure could be significant. The thin hard coating's strength under high frequency loading has been investigated using special specimens, such as coated cantilevers which are excited at resonance frequency [1, 2]. However, it is reasonable to conduct such investigations on real coated parts, as the substrate dynamic response significantly influences the developed stress, strain, strain rate fields in the coating and thus its fatigue behavior [3]. Moreover, the application of real coated parts is imperative due to fact that the film adhesion affects its performance and depends on the substrate properties and treatment before the film deposition [4].

For enabling impact loads on coated specimens originating from real parts of cemented carbide, hardened steel or other materials, a new impact tester with adjustable force data was developed. The surface response of a coated cemented carbide specimen at constant load amplitude and various repetitive impact and signal times is demonstrated in figure 1. In these experiments a permanent substrate plastic deformation develops during the coating - substrate relaxation between two successive impacts, whereas the film is only elastically stressed [5]. On one hand, the imprint diameter between ball indenter and coated surface grows, when the impact time IT increases from 2.5 ms up to 5 ms. On the other hand, the augmentation of the

force signal time ST, as for example up to 20 ms, does not influence the impression diameter. These results are attributed to strain, strain rate depended substrate material properties which affect the contact area between the ball indenter and the coated specimen as well as the developed strain and strain rate fields in both coating and substrate.

In the described investigations, impact tests of various load patterns were conducted on coated cemented carbide inserts. Considering these experimental results, an impact load of certain impact time and amplitude corresponds to a quasi static equivalent one imposing the same remaining imprint depth. In this way, impact loads leading to film fatigue failure after one million impacts also correspond to equivalent static ones. For these equivalent loads, considering substrate and coating elastic – plastic properties, the maximum and remaining surface deformations during loading and coating – substrate relaxation respectively were estimated via FEM – supported calculations. Finally, fatigue critical strain - strain rate combinations were analytically quantified, taking into account the time course of the applied impact force.

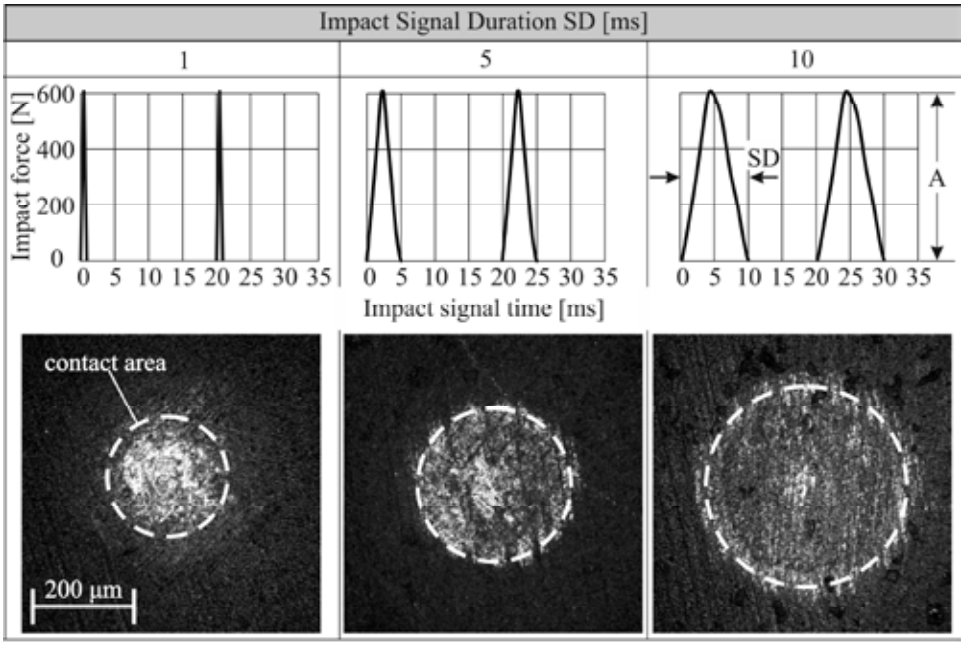

Impact force amplitude A: 600 N, 10^6 impacts, Coating: $Ti_{40}Al_{60}N$,
Substrate:HW/ K05-K20, ball indenter HW/K05-K20, d=5 mm

Figure 1: Imprint diameter on coated inserts at constant load amplitude and various impact and force signal times.

2. EXPERIMENTAL DETAILS

2.1. Substrate and coating

In the described investigations, a Ti40Al60N film was applied. This PVD film was deposited by an industrial CC 800/9 coating unit of CemeCon AG on cemented carbide inserts of SPGN/HW K05-K20 ISO specifications. The hardmetal substrates were polished and micro-blasted before the coating deposition for attaining an improved film adhesion [4].

For determining the mechanical properties of the coating and its substrate at quasi static loads, nanohardness measurements were conducted by a Fischerscope H100 nanoindentation device. The related nanoindentation results are illustrated in figure 2a. The moving average of the measured maximum indentation depth versus the number of conducted measurements is

exhibited in figure 2b. This moving average is stabilized in the case of present specimens' surface roughness approximately after 15 measurements. The reason of this behaviour is thoroughly investigated in reference [6]. Taking into account the actual Berkovich indenter tip form deviations due to its manufacturing imperfections [7], the stress-strain curves of the substrate and film materials were determined by a FEM supported evaluation of nanoindentation's results, as it is described in the literature [6] (see figure 2c). The Young's modulus, the yield and rapture stress of the coating and its substrate are displayed in the table at the figure bottom. The residual stresses which may be induced by the PVD process, thermal or mechanical treatments as for instance by annealing or micro-blasting affect the material mechanical strength [8, 9]. The presented material stress strain curves consider the effect of residual stresses; they are employed in the FEM calculations for estimating the remaining imprint depth after an impact amplitude and time corresponding to an equivalent quasi static load.

The coated surfaces before and after the impact tests were captured by 3D measurements using the confocal system μSURF of NANOFOCUS AG. The coating thickness of approximately 3 μm was determined by ball cratering test.

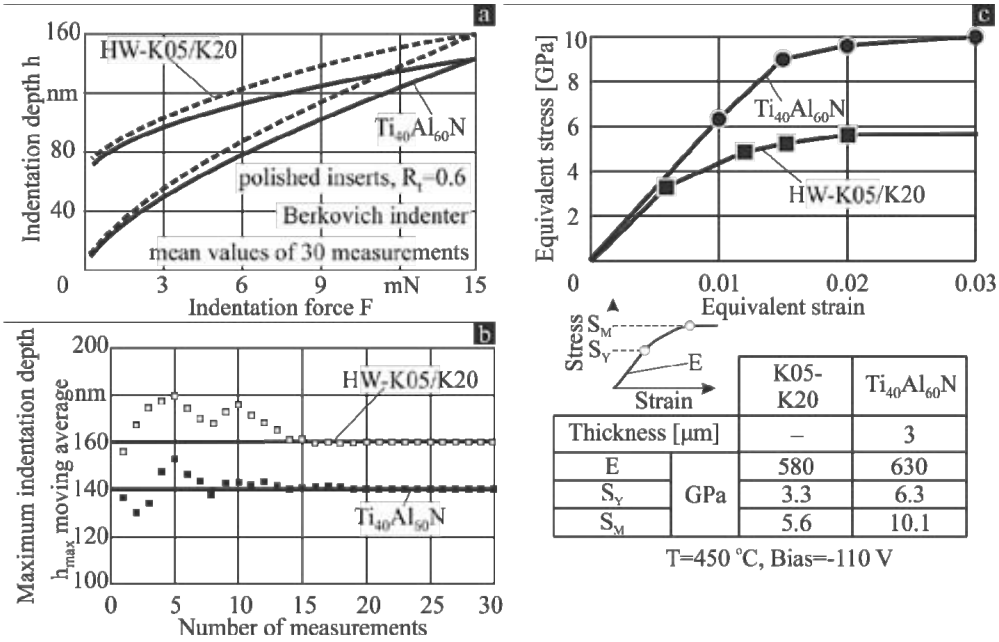

Figure 2: a: Nanoidentation results on the applied substrate and coating,
b: Stabilization of indentation depth after ca. 15 measurements,
c: Determined stress-strain curves of the applied coating and substrate based on nanoidentation results.

2.2. Development of an impact tester with adjustable force pattern

The developed impact tester arrangement is exhibited in figure 3. It consists of a rigid base, a linear drive and a XY table for adjusting the specimen position in relation to the actuator. A piezoelectric force transducer is used for the impact load signal measurement. For generating the impact load, a piezoelectric actuator of a maximum tip displacement of 180 μm and an impact force capacity up to 4500 N was employed. A programmable control unit renders possible the adjustment of the actuator's tip displacement versus time for attaining various force

signal patterns. The hardmetal oscillating ball indenter is moved by the actuator's linear drive towards the specimen, until it contacts its surface. Then, the load amplitude is adjusted by controlling the intender tip displacement. The force transducer and tip displacement signals versus time are transferred to an analog to digital converter and subsequently to a computer for further processing.

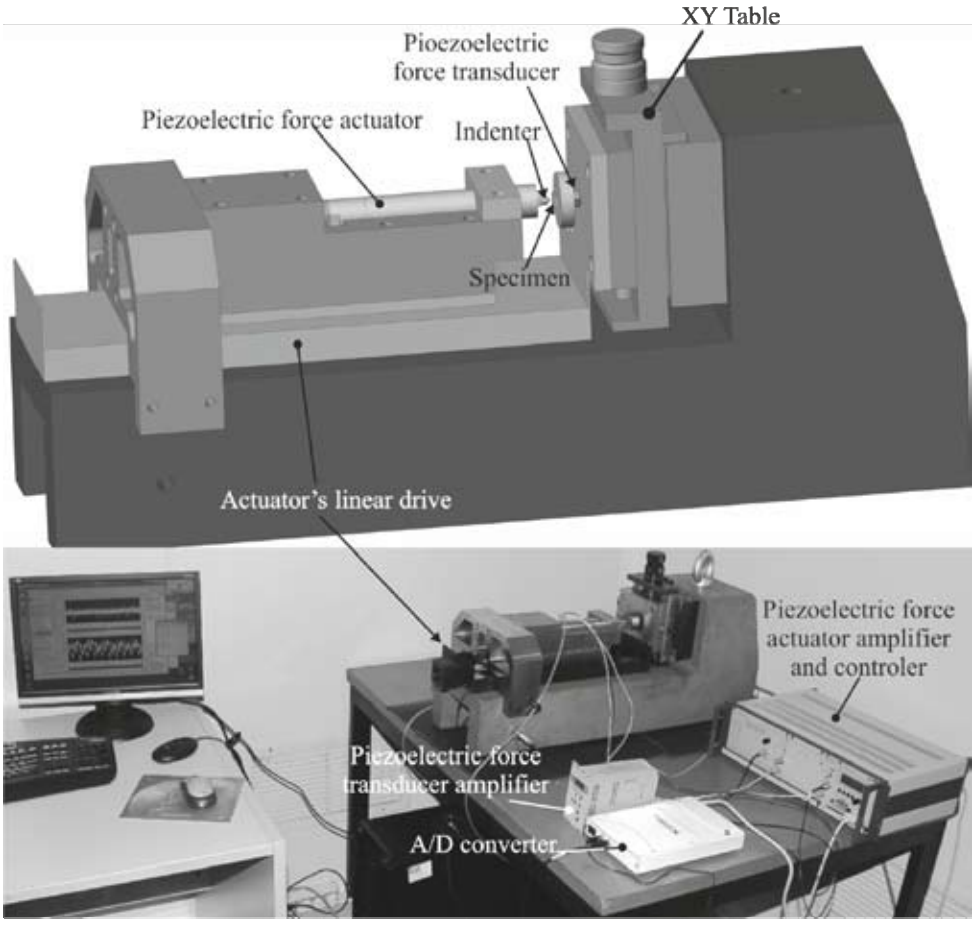

Figure 3: The developed impact tester arrangement with adjustable force pattern.

Figure 4 exhibits force signal patterns and the related adjustable parameters that can be generated by two kinds of actuators, an electromagnetic and a piezoelectric one. The first actuator is driven by Laplace magnetic forces, developed in an electromagnetic field [10, 11]. The signal duration ST of an electromagnetic actuator is approximately 1 ms long, whereas the impact time IT amounts to ca. 0.3 ms. ST and IT are not adjustable parameters and depend on the impact tester spindle constructive details as well as on the ball indenter and specimen material strength properties. In contrast, the piezoelectric actuator enables the realization of various impact force signal patterns (sinusoidal, triangular, trapezoidal etc.) with different amplitudes, durations and frequencies. In the described investigations, due to the technical specifications of the applied piezoelectric force actuator, it was not possible to apply impact times shorter than 2 ms at force amplitudes larger than ca. 60 daN. Such test conditions were conveniently implemented by the electromagnetic force actuator.

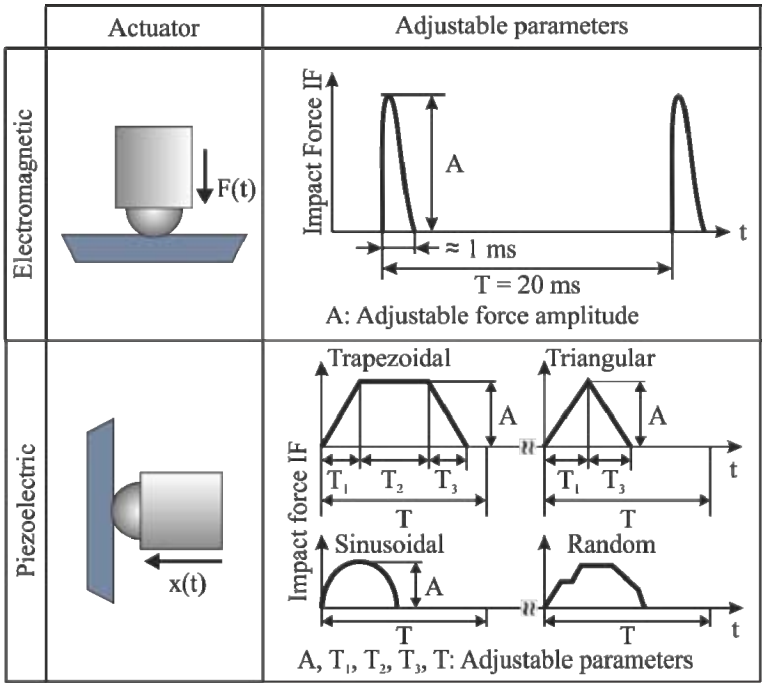

Figure 4: Adjustable force signal's parameters of various force actuators.

3. NUMERICAL METHODS

The axisymmetric FE model for calculating the coated surface response at quasi static loads was developed on the platform of the ANSYS software [12]. This model is exhibited in figure 5 as well as the boundary conditions and the finite element discretization network. For meshing the two dimensional geometry of the carbide ball, coating and substrate plane elements were selected. A large number of approximately 25000 elements was generated. Contact elements were used for describing the interface between the ball indenter and the coating, whereas the friction coefficient was set equal to 0.1. A Y-axis restrain was applied to the nodes located at the bottom surface of the substrate. The induced coating and substrate deformation by the slow penetration of the carbide ball into the film was determined at predescribed indentation depths. The FE model dimensions, material properties, boundary conditions, number of elements etc., are changeable parameters for achieving a flexible and reproducible model. In such three-dimensional stress–strain problems, the material status is oriented by the position of the principal stress vector relative to the yield surface. In general, two hardening rules are available; the isotropic and the kinematic one [13]. In the first case the yield surface remains centered around its initial center and expands in size as the plastic strain develops. Moreover, the kinematic hardening assumes that the yield surface remains constant in size and the surface translates in stress space with progressive yielding, whereas the Besseling model is used [13, 14], also called sub-layer or overlay model, to characterize the material behavior. The FEM model developed in the frame of the present paper was solved for both plasticity models and the corresponding results were almost identical. Considering that the kinematic hardening rule leads to a rapid convergence in the corresponding FEM calculations, this feature was applied in the described investigations.

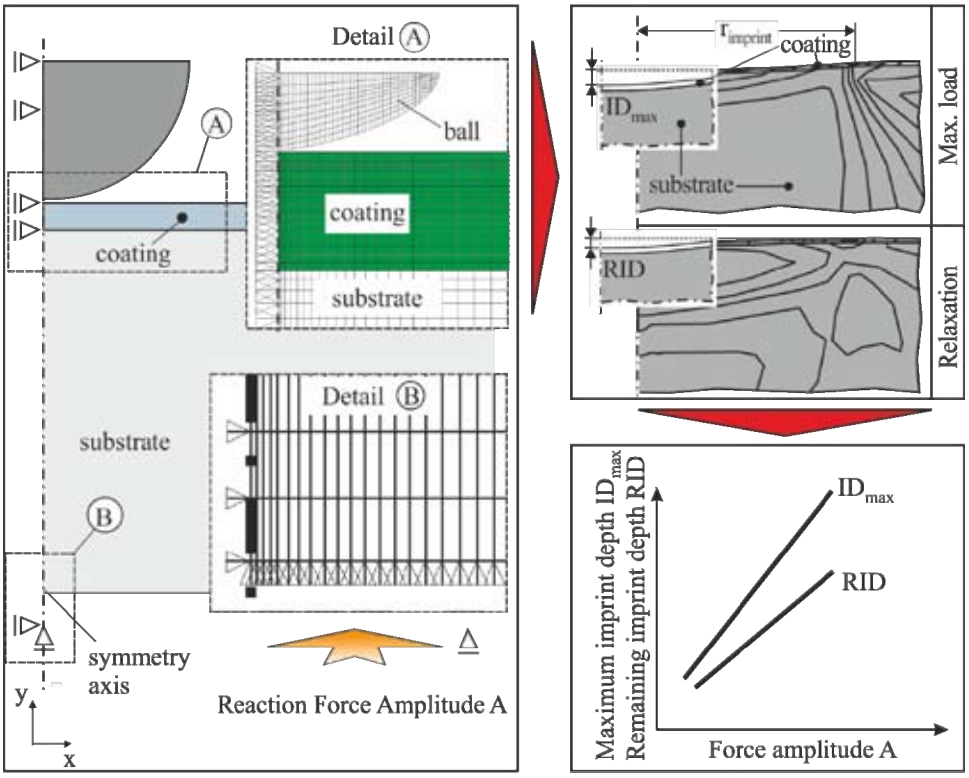

Figure 5: The developed FE - model for calculating maximum and remaining surface deformation at quasi static loads.

By the introduced FEM – model the maximum indentation depth IDmax, and the remaining imprint depth RID after the coating relaxation can be determined versus the reaction force amplitude A (see Figure 5). Considering the attained experimental results which will be presented in the next sections, quasi static calculations are valid for impact durations larger than 10 ms, since over this time the coated surface response is practically indentical with that one at the equivalent static load.

4. RESULTS AND DISCUSSION

4.1. Film and substrate deformation at various impact force durations and amplitudes.

The impact test has been successfully applied for characterizing, among others, PVD films fatigue [5, 11]. In this test, the coating deforms elastically and the substrate elastoplastically, depending on the impact load. The coating damage initiation is mainly induced by fatigue mechanisms, leading to a gradual removal of film segments in the contact area between the ball indenter and the specimen at highly superficially loaded regions [15]. In general, after the film damage initiation a steep coating fracture and removal develops [16]. In the conducted investigations, at the applied impact test conditions after 10^4 impacts no kind of film failure has been developed. All investigations were conducted two times on individual specimens. The scatter of the remaining imprint depth measurements was almost always less than 5%. In cases of larger deviations, a further test and related measurements were carried out and the related mean value was considered. Measured crater depths are demonstrated in figure 6a. These results were attained at a force amplitude of 140 daN and impact signal durations of 0.3 ms,

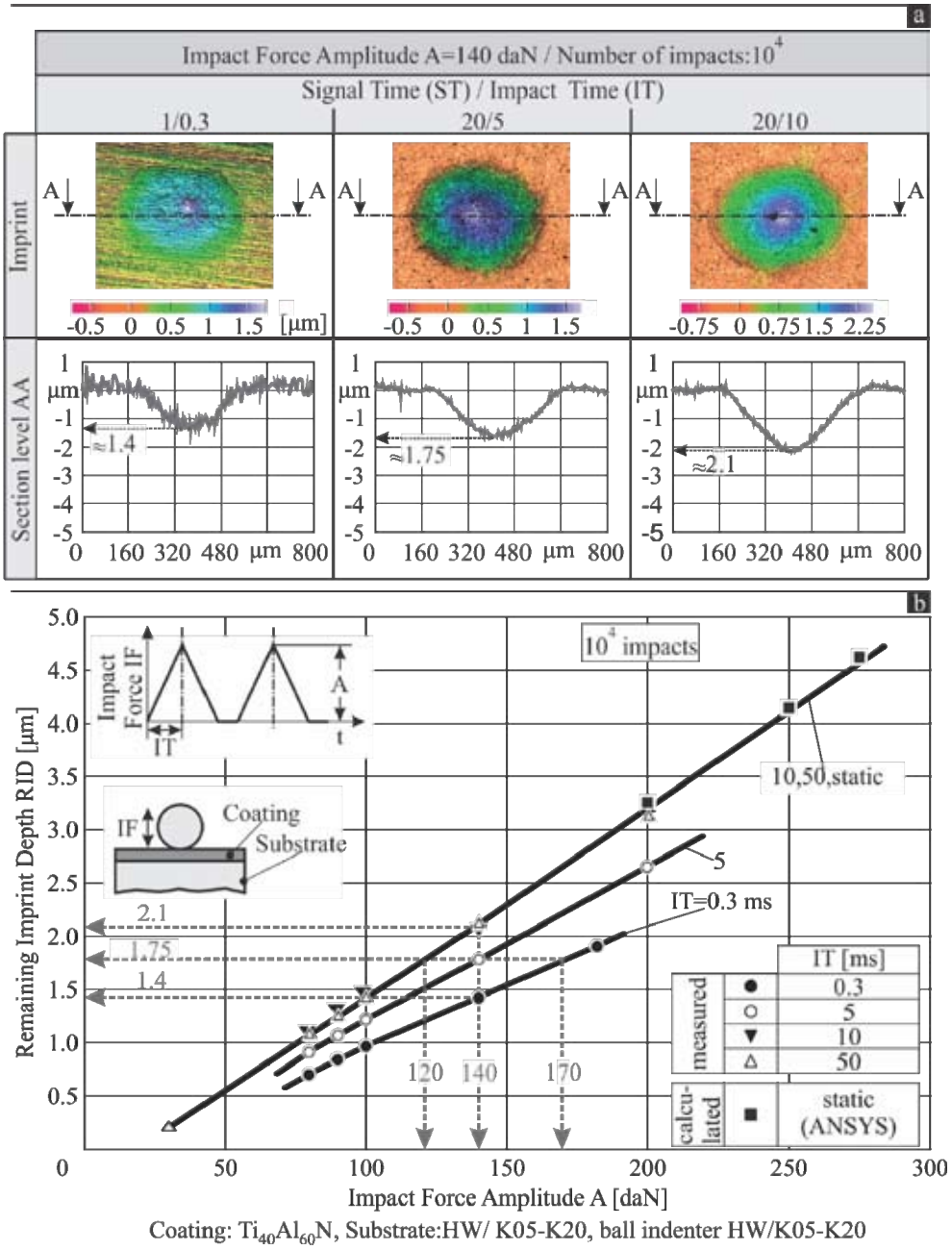

Figure 6: a: Remaining imprint depths by confocal measurements determined,
b: Experimental and FEM calculated remaining imprint depths at various impact conditions.

5 ms and 10 ms. The remaining imprint depth (RID) increased from 1.4 μm up to 1.75 μm and 2.1 μm respectively. The determined RIDs versus the impact force amplitude are monitored in figure 6b. RID increases, as the impact time grows at the same force amplitude. In Figure 6b, the FEM calculated remaining imprint depths at various static loads are also exhibited. According to these results, the impact duration effect on the coating – substrate deformation and thus on the developed remaining impact depth is negligible at impact times IT longer than 10 ms. In this way, the related RIDs at impact times larger than 10 ms, are practically identical to the corresponding ones of the static load case. Thus, results at impact times larger than 10 ms are accurately described by the FEM calculated ones at the same force amplitudes. Hence, it can be stated that the same impact load lead to comparable larger coating – substrate plastic deformations and remaining imprint depths as well, at longer impact times. At the applied experimental conditions, this is valid, up to an impact time of 10 ms. Over this duration the coated surface deformation can be associated to that one, at a quasi static load. For example, at impact times less than 10 ms, for attaining a remaining imprint depth of 1.75 μm, the force amplitude of 120 daN in a quasi static loading case has to be increased up to 140 daN and 170 daN, at impact times of 5 ms and 0.3 ms respectively (see figure 6b). This tendency can be explained by material hardening effects at high frequencies excitation, i.e. at a shorter impact time [17, 18, 19]. The displayed in figure 6 remaining imprint depths in various load cases will be taken into account for determining the coating failure depth developed during the impact test, as it will be introduced in the next section.

4.2. Film fatigue fracture at various impact durations and amplitudes.

The coating fatigue fracture was investigated at various impact force amplitudes after 10^6 impacts. Characteristics results concerning the developed imprint depths at various impact force amplitudes are presented in figure 7. The applied force signal possessed triangular pattern with constant growth duration (impact time IT) of 0.3 ms. For detecting the part of the remaining imprint depth which corresponds to the developed substrate remaining plastic deformation, impact tests at a restricted number of 10^4 impacts were also conducted. At this number of impacts, as it is already mentioned, no kind of film failure in all investigated cases occurred. It is evident, that at an impact load amplitude of 80 daN, the imprints after 10^4 and 10^6 impacts are almost identical, i.e. no film damage develops. At the larger impact load of 90 daN, the remaining imprint depth after 10^6 impacts is slightly larger than the corresponding one at 10^4 impacts. This is caused by micro fatigue mechanisms on the film surface, initiating the film fracture and removal [15, 16]. The difference between the related remaining imprint depths corresponds to the coating failure depth CFD which in the present case amounts to approximately 0.5 μm. Finally, at an impact force amplitude of 100 daN, the coating fatigue endurance is exceeded and CFD approximates the coating thickness of 3 μm. In this case, the overall developed imprint depth amounts to ca. 4 μm, i.e. it corresponds to the removed coating thickness of ca. 3μm, plus the substrate remaining plastic deformation, which at the applied impact load amounts to about 1 μm. The latter can be estimated with the aid of Figure 6b, at an impact force amplitude of 100 daN and impact time IT of 0.3 ms.

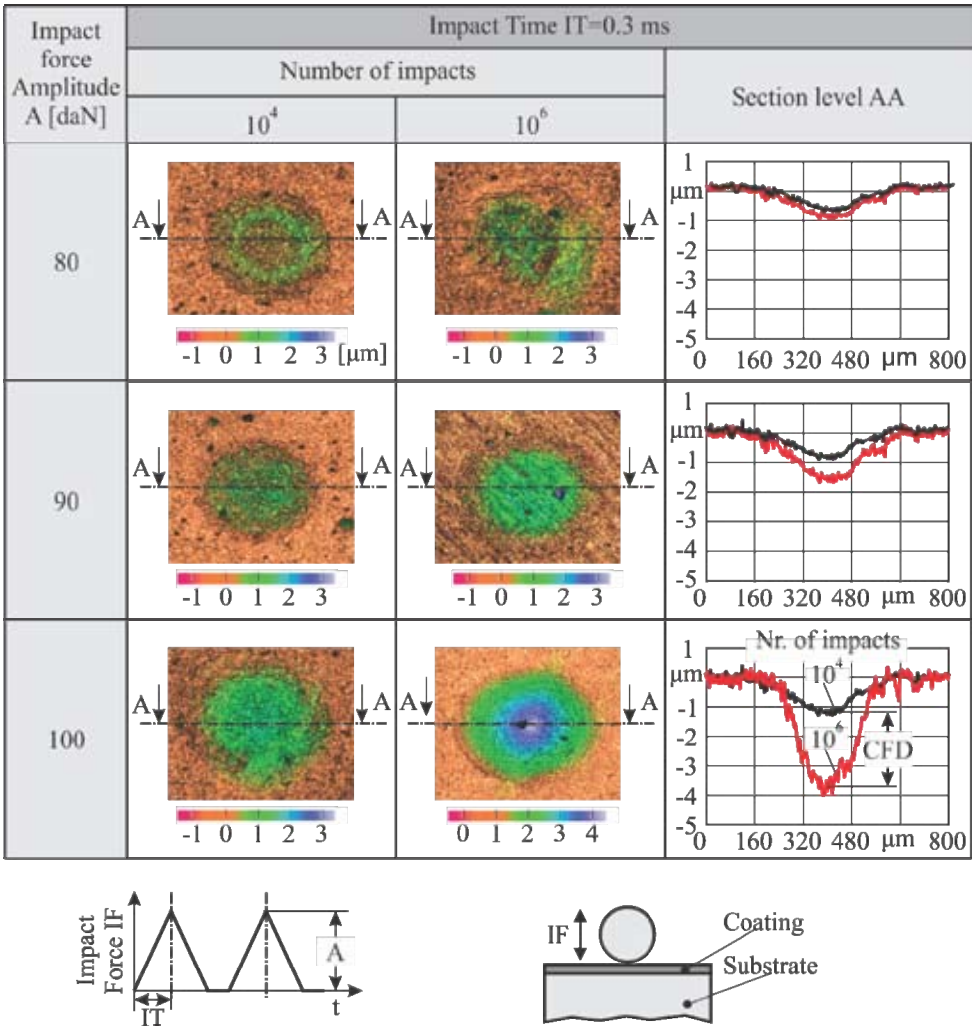

Figure 7: Coating Failure Depth (CFD) determination based on imprint geometries by 3D confocal measurements captured.

Figure 8 displays the measured remaining imprint depths at various impact force amplitudes and times after 10^6 impacts. The remaining imprint depth after one million impacts significantly increases versus the force amplitude, at all impact durations. Moreover, as the impact time grows, the same remaining imprint depth develops at comparably higher impact force amplitudes. The film fatigue fracture after 10^6 impacts can be quantified by the coating failure depth CFD which is introduced in figure 7. Related results versus the force amplitude are illustrated in figure 8b. The curves of this figure are determined by subtracting RID_4 associated to the remaining plastic deformation of the coated specimen surface, developed at the same force amplitude however after only 10^4 impacts (see Figure 7), from the remaining imprint depth RID_6after one million impacts (see figure 8a). According to figure 8b, the film fatigue fracture is initiated at impact force amplitudes of approximately 90 daN, 160 daN and 195 daN, at impact times of 0.3 ms, 5 ms and 10 ms respectively. Hereupon, as coating fatigue fracture initiation

criterion at a certain force amplitude, a coating failure depth CFD of 0.5 µm after one million impacts was considered. The coating fatigue fracture after one million impacts develops at lower force amplitudes, as the impact time IT diminishes. This happens since at short impact durations, dislocation concentrations develop in the coating material, leading to faster crack propagation and thus to film fatigue fracture [18].

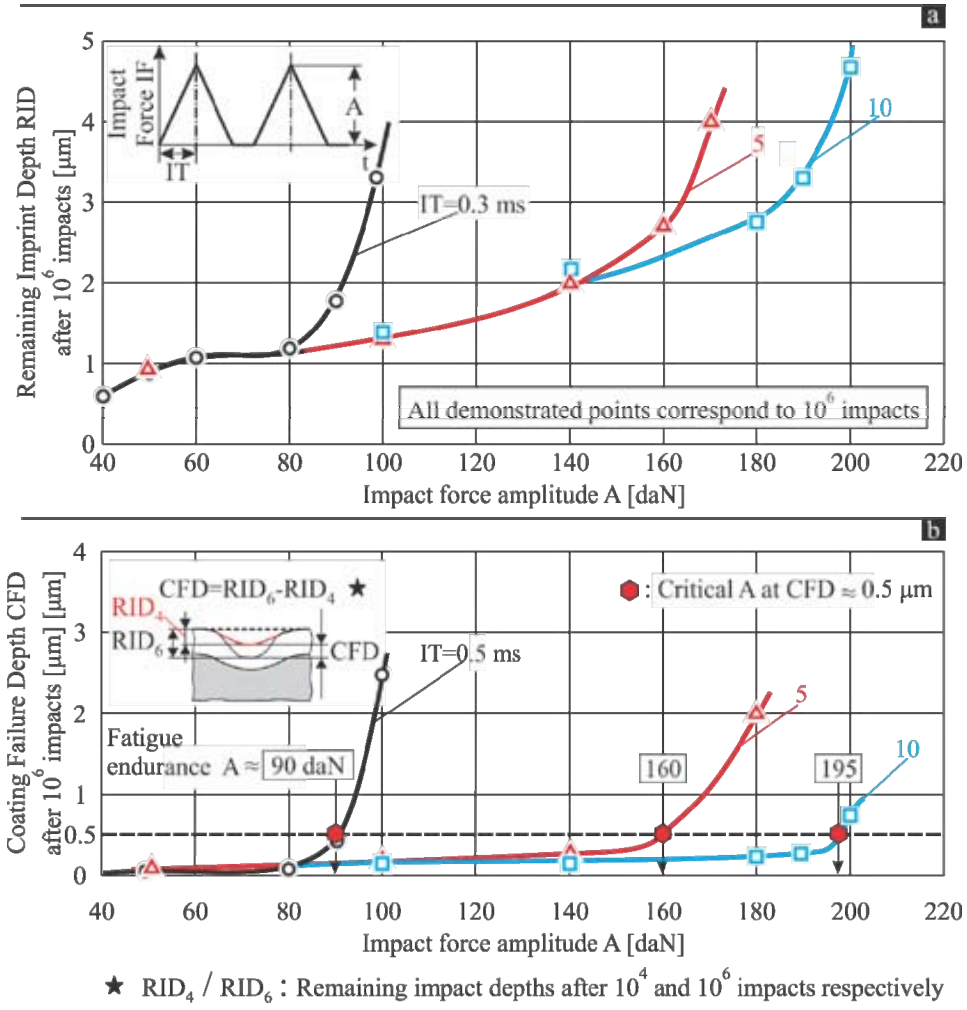

Figure 8: a: Remaining imprint depths versus the impact force after one million impacts at various impact times,
b: Coating failure depth at various impact times and amplitudes after one million impacts.

5. FEM SUPPORTED CALCULATION OF FILM FATIGUE CRITICAL STRAIN, STRAIN RATE COMBINATIONS

For determining the developed strain fields in the film and substrate materials during the indenter ball penetration into the coated specimen at quasi static loads, the FEM – supported procedure described in figure 5 was employed. In this FEM simulation, impact times longer than 10ms were taken into account, since over this time the strain rate effect on the film and substrate deformation and thus on the developed strain field is negligible (see figure 6b). In the conducted FEM calculations, the coating and substrate material stress strain laws introduced in figure 2c were used. For considering the effect of the impact force duration on the developed strain field, as it is already described, it was assumed that impact loads of various amplitudes and times inducing equal remaining imprint depths cause the same substrate deformations during the ball indenter penetration. The way of corresponding an impact force amplitude of various durations IT to a maximum IDmax and remaining RID is explained in figure 9. The experimentally determined remaining imprint depths (RID) at an impact duration t_i shorter or larger than 10ms are monitored versus the impact force amplitude A. The RIDs associated to impact times IT larger than 10 ms are also corroborated by FEM calculations. Employing this method, at a certain impact force amplitude and impact time, the equivalent static loading case can be determined and furthermore the associated developed strain field as well.

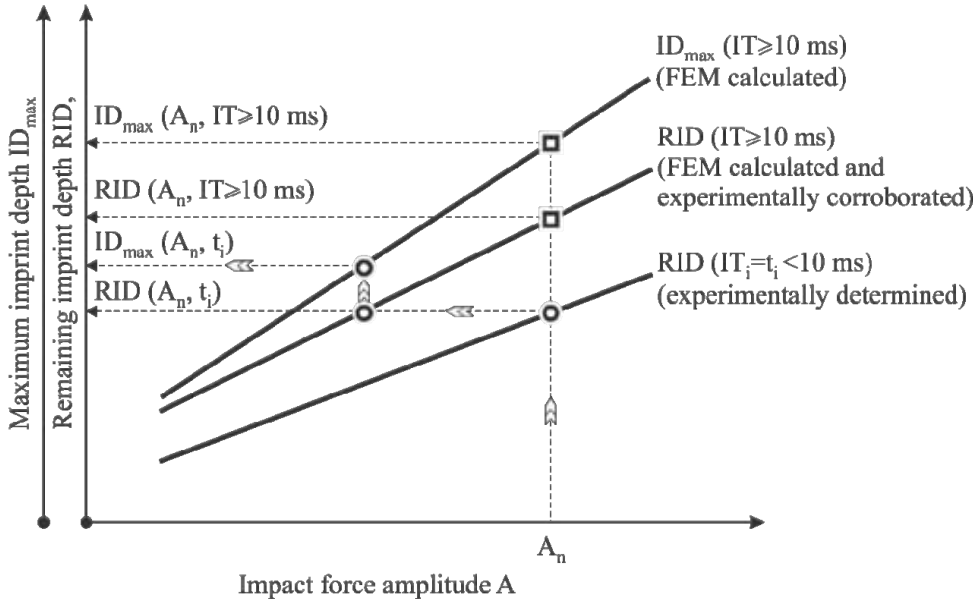

Figure 9: Determination of maximum and remaining imprint depths dependent on the impact force amplitude A, at impact times longer or shorter than 10 ms.

A related example is displayed in figure 10. As the ball indenter penetrates slowly into the coated specimen, the film von Mises strain at the most stressed imprint vicinity position CE grows. As representative strain value in this location at the maximum equivalent static load, the von Mises strain average at the three end nodes of the ball indenter – coated specimen contact and at a depth from the film surface of approximately 0.6 µm was considered.

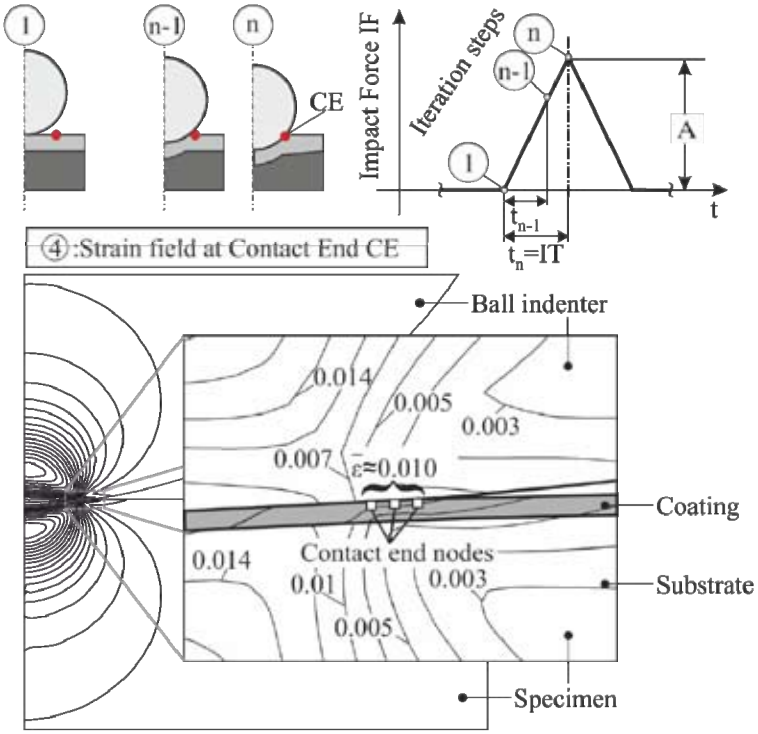

Figure 10: FEM calculated strain field in the contact region between ball indenter and coated specimen at quasi static loading and maximum penetration depth.

This representative strain is plotted versus the impact force amplitude at various impact times (see figure 11). As it was expected, the strain at constant impact force amplitude increases as the impact time IT grows. Moreover, based on the force amplitudes which initiate fatigue fracture at various impact times and have already monitored in figure 8, the corresponding von Mises strains are also displayed in figure 11. These fatigue critical von Mises strains ε_f correspond to certain impact amplitudes and time combinations.

The fatigue endurance strain ε_f is illustrated versus the impact time IT in figure 12. As it is already explained, the fatigue endurance strain ε_f increases as the impact time grows. For determining ε-$\dot{\varepsilon}_f$ combinations insuring film fatigue endurance after one million impacts, the strain rates difference developed at CE in the iteration steps n-1 and n (see figure 10) were calculated. Considering the iteration step interval time (t_n - t_{n-1}), the strain rate f corresponding to a fatigue endurance strain ε_f at CE can be determined as following:

$$\dot{\varepsilon}_f = \frac{d\varepsilon_f}{dt} \approx \frac{\Delta\varepsilon_f}{\Delta t} = \frac{\bar{\varepsilon}_n - \bar{\varepsilon}_{n-1}}{t_n - t_{n-1}} \quad (1)$$

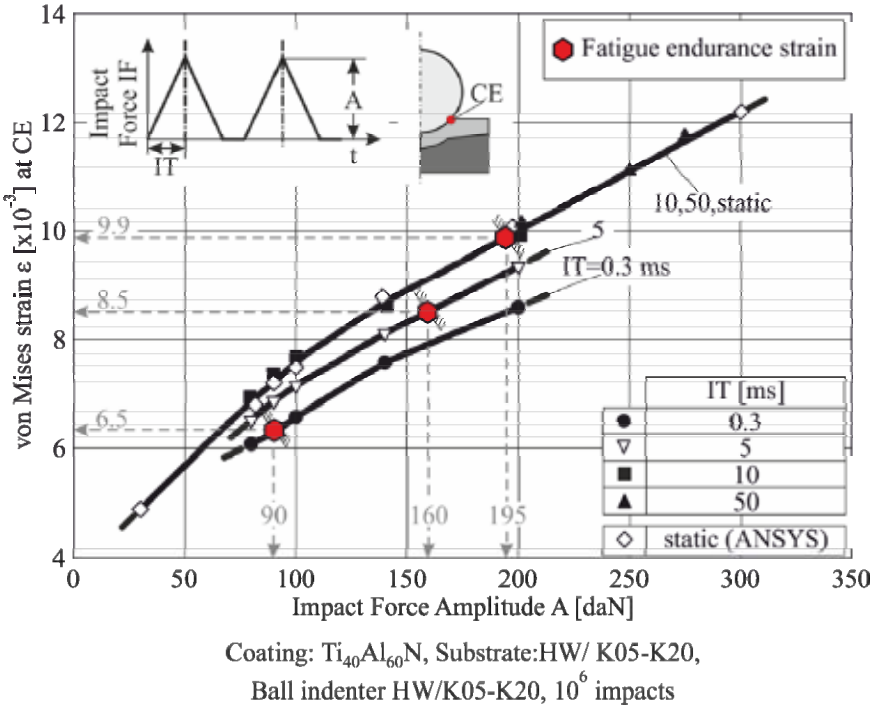

Figure 11: FEM-calculated equivalent strains at CE versus the impact force amplitude at various impact times.

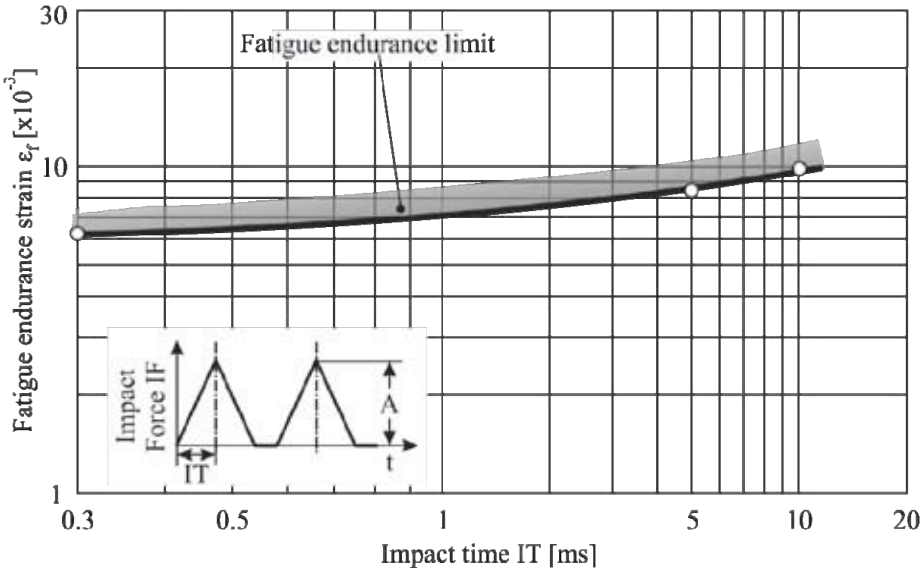

Figure 12: Fatigue endurance strain ε_f at various impact times.

Characteristic calculations' results of fatigue critical strain ε_f, strain rate $\dot{\varepsilon}_f$ combinations are displayed in figure 13. In the FEM calculations of this example, one hundred iteration's steps were carried out. It is evident that a strain rate $\dot{\varepsilon}_f$ augmentation leads to fatigue endurance strain ε_f decrease. According to the film stress strain diagram presented in figure 2c, three strain regions are distinguished. The first one up to a strain of 0.01 is associated with film pure elastic deformation. Moreover, in a strain range between 0.01 and 0.015, a quasi elastic coating deformation develops. Strains larger than 0.015 lead to film plastic deformation. The determined fatigue endurance ε_f at strain rates $\dot{\varepsilon}_f$ less than approximately 2 s^{-1} (see figure 13) enter into the quasi elastic film deformation region 2. It is considerable that strain rates larger than ca. 2.5 s^{-1} impose coating fatigue failure already at a strain of approximately $10*10^{-3}$, whereas at an only 35% smaller strain of $6.5*10^{-3}$, the corresponding fatigue endurance strain rate is almost 12.4 times larger amounting to ca. 31 s^{-1}. The displayed data of the investigated TiAlN coating can be used for film fatigue considerations in various applications as for example in interrupted cutting with coated tools [20].

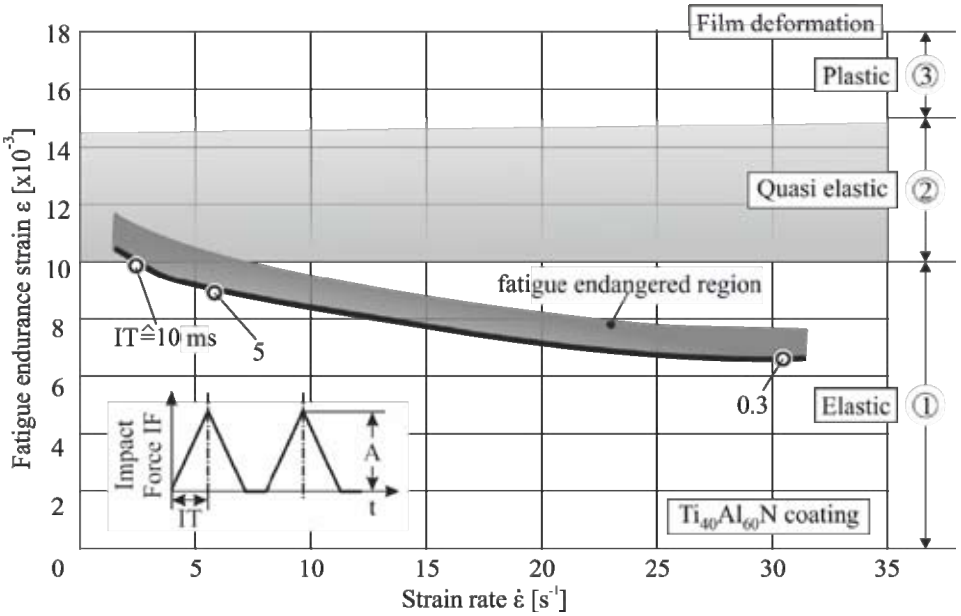

Figure 13: Coating fatigue endurance strain ε_f versus strain rate $\dot{\varepsilon}_f$.

6. CONCLUSIONS

Strain rate effects on coated surfaces' response and their film fatigue fracture initiation were investigated by a developed impact tester which facilitates the impact force signal pattern modulation. Employing the introduced methods, the film fatigue fracture initiation was detected, dependent on the impact force amplitude and duration. Based on these results and appropriate FEM calculations, fatigue endurance strain ε_f, strain rate $\dot{\varepsilon}_f$ combinations were determined. Theseε_f, $\dot{\varepsilon}_f$ combinations reveal that slight strain ε_f augmentation can lead to significant reduction of the permit able strain rate $\dot{\varepsilon}_f$ for avoiding film fatigue fracture. The attained data can be used for explaining failure mechanisms of coatings subjected to cyclic impact loads in various applications.

7. REFERENCES

1. S. Burger, C. Eberl, A. Siegel, A. Ludwig, O. Kraft, A novel high-throughput fatigue testing method for metallic thin films, Sci. Technol. Adv. Mater 12 (2011) 054202.
2. G.P. Zhang, C.A. Volkert, R. Schwaiger, R. Mönig, O. Kraft, Fatigue and thermal fatigue damage analysis of thin metal films, Microelectron. Reliab. 47 (12) (2007) 2007-2013.
3. K. –D. Bouzakis, M. Batsiolas, G. Malliaris, M. Pappa, E. Bouzakis, G. Skordaris, New methods for characterizing coating properties at ambient and elevated temperatures, Key Eng. Mat. 438 (2010) 107-114.
4. K.-D. Bouzakis, A. Asimakopoulos, G. Skordaris, E. Pavlidou, G. Erkens, G., The inclined impact test: A novel method for the quantification of the adhesion properties of PVD films, Wear (2007) 262 (11-12) 1471-1478.
5. K.-D. Bouzakis, N. Vidakis, T. Leyendecker, G. Erkens, R. Wenke, Determination of the fatigue properties of multilayer PVD coatings on various substrates, based on the impact test and its FEM simulation, Thin Solid Films 308-309(1997), Issue 1-4, 315-322.
6. K.-D. Bouzakis, N. Michailidis, S. Hadjiyiannis, G. Skordaris, G. Erkens, The effect of specimen roughness and indenter tip geometry on the determination accuracy of thin hard coatings stress-strain laws by nanoindentation, Mater. Charact. 49 (2) (2002) 149-156.
7. K.-D. Bouzakis, N. Michailidis Indenter surface area and hardness determination by means of a FEM – supported simulation of nanoindentation, Thin Solid Films 494 (2006), 155-160.
8. K.-D. Bouzakis, G. Skordaris, J. Mirisidis, S. Hadjiyiannis, J. Anastopoulos, N. Michailidis, G. Erkens, R. Cremer, Determination of coating residual stressalterations demonstrated in the case of annealed films and based on a FEM supported continuous simulation of the nanoindentation, Surface and Coatings Technology 2003, 174/175, 487-492.
9. K.-D. Bouzakis, G. Skordaris, F. Klocke, E. Bouzakis, A FEM-based analytical–experimental method for determining strength properties gradation in coatings after micro-blasting, Surface and Coatings Technology 2009, 203, 2946-2953.
10. O. Knotek, B. Bosserhoff, A. Schrey, T. Leyendecker, O. Lemmer, S. Esser, A new technique for testing the impact load of thin films: The coating impact test, Surf. Coat. Tech. 54/55 (C) (1992) 102–107.
11. K.-D. Bouzakis, N. Michailidis, A. Lontos, A. Siganos, S. Hadjiyiannis, G. Maliaris, G. Giannopoulos, Characterization of cohesion, adhesion and creep-properties of dynamically loaded coatings through the impact tester, Z. Metallkd. 92 (10) (2001) 1180-1185.
12. Swanson Analysis System, INC.,ANSYS user manual, Vol. 1 Theory, Vol. 2 Procedures, Vol. 3., Volume 4 Commands (2004).
13. J.F. Besseling, E. Van Der Giessen, Mathematical Modelling of Inelastic Deformation, Chapman & Hall (1994) ISBN 0412452804
14. J.L. Loubet, J.M. Georges, G. Meille, Vickers Indentation Curves of Elastoplastic Materials, Microindentation Techniques in Material Science and Engineering, ASTM STP 889, Philadelphia (1986) 72–89.
15. Bouzakis K.-D., Siganos A. Fracture initiation mechanisms of thin hard coatings during the impact test. Surface and Coatings Technology. 2004; 185(2-3): 150-9.
16. Bouzakis K.-D., Siganos A., Leyendecker T., Erkens G., Thin hard coatings fracture propagation during the impact test, Thin Solid Films 460 (2004), 181-189.
17. B.L. Boyce, M.F. Dilmore, The dynamic tensile behavior of tough, ultrahigh-strength steels at strain-rates from 0.0002 s^{-1} to 200 s^{-1}, Int. J. Imp. Eng. 36 (2) (2009) 263-271.
18. L.E. Murr, Metallurgical effects of shock and high-strain-rate loading, in: T.Z. Blazynski (Ed.), Materials at high strain rates, Elsevier, Essex (England), 1987, pp. 1–46.
19. J. Harding, The effect of high strain rates on material properties, in: T.Z. Blazynski (Ed.), Materials at high strain rates, Elsevier, Essex (England), 1987, pp. 133-186.
20. K.-D. Bouzakis, S. Makrimallakis, G. Katirtzoglou, E. Bouzakis, G. Skordaris, G. Maliaris, S. Gerardis, Coated tools' wear description in down and up milling based on the cutting edge entry impact duration, CIRP Annals (2012), 115-118.